Iraqi Journal of Physics, 2026
https://doi.org/10.30723/ijp.v24i3.1620
Vol.24, No.3, PP.88-100
P-ISSN: 2070-4003
E-ISSN: 2664-5548

Nuclear Structure and Deformation Characteristics of Neutron-Deficient $^{180\text{-}192}$Hg Isotopes using the Skyrme–Hartree–Fock Method

Luma J. Abbas[1*]
[1]*College of Energy and Environmental Science, Al-Karkh University of Science, Baghdad, Iraq*
[*]Corresponding author: Lumaa.jamal@kus.edu.iq

Abstract
This study investigates the ground-state nuclear structure of neutron-deficient mercury (Hg) isotopes in the mass number range A=180-192 within the self-consistent Skyrme-Hartree-Fock (SHF) framework using different parametrizations. The even-even and odd-even A members of the isotopic chain were examined in terms of nuclear deformations, charge radii, binding energies, separation energies, and nuclear density distributions. The calculated charge radii agreed with the experimental systematics, with residual deviations below 0.082 fm, confirming the quantitative reliability of the SHF in describing nuclear spatial observables. Furthermore, the nuclear charge-density distributions calculated using the Skyrme Skxcsba parameterization showed good agreement with the available experimental data, exhibiting central densities of approximately $\rho_{ch} \approx 0.06–0.07$ fm^{-3} and a systematic outward shift with increasing mass number. The nuclear matter-density profiles confirm central saturation near $\rho_{\circ} \approx 0.16$ fm^{-3}, together with a gradual broadening of the surface diffuseness region toward the heavier isotopes, consistent with the increasing nuclear size. The axial quadrupole potential energy surfaces (PESs) were mapped as a function of the deformation parameter β_2 for all the investigated isotopes. The resulting surfaces revealed a transition from weakly oblate to prolate configurations near the neutron mid-shell region.

Article Info.

Keywords:
Hg Isotopes, Shape Coexistence, Skyrme–Hartree–Fock, Quadrupole Deformation, Neutron Skin.

Article history:
Received: Jun. 20, 2026
Revised: Aug. 10, 2026
Accepted: Aug. 16, 2026
Published: Sep. 01, 2026

1. Introduction
The nuclear structure of neutron-deficient Hg isotopes is characterized by a complex interplay of competing collective modes, leading to the well-known phenomenon of shape coexistence in the region near the N = 104 neutron mid-shell. This behavior results from competition between the stabilizing effect of shell closures and the collective correlations that favor prolate and near-spherical configurations.

The structure evolution of Hg isotopes is essentially governed by the interplay between the spherical shell effects associated with their proximity to the Z = 82 proton shell closure and the quadrupole collectivity induced by the gradual filling of mid-shell neutron orbitals when approaching the neutron number N = 104. The mercury isotopic chain is a well-known example of nuclear shape coexistence, owing to the presence of energetically competitive prolate, oblate, and near-spherical states [1].

The self-consistent Hartree-Fock (HF) framework, when coupled with the Skyrme energy density functional, stands among the most extensively employed theoretical tools for probing the structural evolutions of Hg isotopes. Ground-state properties within this scheme emerge from minimizing the total HF energy with respect to the nuclear density distribution, with deformation and pairing correlations incorporated self-consistently throughout. The Skyrme functional was extensively tested against experimental data. It can reproduce features that are fundamental for finite nuclei and nuclear matter, like binding energies, charge radii and deformation properties. This makes it a reliable tool for studying isotopic trends for a large variety of nuclei [2].

Advances in nuclear energy density functionals have extended the theoretical facility beyond axial-symmetry, enabling systematic investigation of structural properties along isotopic chains that incorporate non-axial deformation [3]. Higher-order extensions of the Skyrme functional further accommodate non-axial and reflection -asymmetric configurations not captured at leading order-refinements particularly relevant to shape coexistence phenomena in Hg-isotopes, where pairing correlations compete with shell effects in determining configurational stability. For highly parameterized interactions like SLy4, the surface energy coefficient is found to be an important factor controlling the deformability of nuclear matter. Better values of these parameters increase the capability of the framework to describe the energy scales of symmetry breaking processes, like transitions between different axial and non-axial configurations. This mutual dependence is important for the mapping of potential energy surfaces, as it assists to make sure that the functional captures the competition among intrinsic configurations in the mercury isotopic chain without overestimating the resistance to deformation [4–6].

This interdependence plays a decisive role in the reliable mapping of potential energy surfaces (PES), as it ensures that the functional reproduces the competition between various intrinsic configurations in the mercury isotopic chain. In particular, this is applicable in regions where the effects of symmetry-breaking contribute strongly to the ground-state structure. This methodological framework offers a pathway toward more dependable extraction of physical observables, including fission barrier heights, given their pronounced sensitivity to the interplay between shell structure and nuclear deformability [6,7]. Beyond this, the marked dependence of these properties on pairing strength underscores its regulatory role in shaping the collective mass parameter, thereby governing the system's effective inertia throughout shape reorganization. Such correlations further modulate the density of states near the Fermi surface, directly affecting the breadth of the transition zone within which the oblate and prolate configurations remain energetically competitive. Hence, the energy spectra are found to be very sensitive to the pairing strength as a function of deformation, especially in the vicinity of the crossing points of competing orbitals [8].

The present work carries out a systematic and Skyrme-Hrtree-Fock (SHF) investigation of the neutron-deficient Hg isotopic chain, spanning the range A = 180–192, employing the SLy4 and SKxcsba parameterizations. The inspection of ground-state deformation parameters and mapping of the axial potential energy surfaces (PES) for both even-even and odd-even A of the chain identify the conditions under which shape coexistence manifests. In addition, the one-neutron and two-neutron separation energies, S_n and $S_{2n,}$ have been evaluated across the full isotopic chain to assess the reproducibility of the odd-even staggering, as well as the evidence of structural transitions or subshell effects. By correlating these complementary structural observables within a unified microscopic framework, the present work seeks to introduce a predictive description of the nuclear structure evolution in neutron-deficient Hg-isotopes, while quantitatively assessing the descriptive and predictive capability of the SHF approach in this transitional mass region. The main objective is to analyze the results for deformation properties, nuclear radii, binding energies, and separation energies, respectively.

2. Theoretical formalism

2.1. Shell Model Calculations

In the neutron-proton formalism adopted by the NUSHELLX code, the Hamiltonian can be expressed as a sum of three distinct terms [9]:

$$H = H_{nn} + H_{pp} + H_{pn} \quad (1)$$

The corresponding second-quantized representation for H_{pn} is given as:

$$H_{pn} = \sum_{pnp'n',J_\circ} \left\{ \left[a_p^+ a_n^+\right]^{J_\circ} \otimes \left[\tilde{a}_{p'} \tilde{a}_{n'}\right]^{J_\circ} \right\}^{(0)} \quad (2)$$

which can recouple the operators to [9]:

$$\left\{ \left[a_p^+ a_n^+\right]^{J_\circ} \otimes \left[\tilde{a}_{p'} \tilde{a}_{n'}\right]^{J_\circ} \right\}^{(0)} = -\sum_{\lambda} \sqrt{(2\lambda+1)(2J_\circ+1)}(-1)^{j_n+j_{p'}-\lambda-J_\circ} \times \begin{Bmatrix} j_p & j_n & J_\circ \\ j_{n'} & j_{p'} & \lambda \end{Bmatrix} \times \left\{ \left[a_p^+ \tilde{a}_{p'}\right]^{\lambda} \otimes \left[a_n^+ \tilde{a}_{n'}\right]^{\lambda} \right\}^{(0)} \quad (3)$$

where $\begin{Bmatrix} \cdot & \cdot & \cdot \\ \cdot & \cdot & \cdot \end{Bmatrix}$ represents 6j- symbol, p represents a single-particle wave function (n_p, ℓ_p, j_p). Furthermore, H_{pn} can be written in the particle-hole form as:

$$H_{pn} = \sum_{pp'nn'\lambda} F_\lambda(pp'nn') \left\{ \left[a_p^+ \tilde{a}_{p'}\right]^{\lambda} \otimes \left[a_n^+ \tilde{a}_{n'}\right]^{\lambda} \right\}^{(0)} \quad (4)$$

where

$$F_\lambda(pp'nn') = -\sum_{J_\circ} \sqrt{(2\lambda+1)(2J+1)}\,(-1)^{n+p'-\lambda-J} \begin{Bmatrix} p & n & J \\ n' & p' & \lambda \end{Bmatrix} \quad (5)$$

The many-particle reduced matrix elements of the electric multipole transition operator $\hat{T}^{\lambda}$ for an n-particle model space wave function of multipolarity λ can be expressed as the sum of the product of one-body density matrix (OBDM) elements times the reduced single-particle matrix elements, which is given as [9]:

$$\left\langle f \left\| \hat{T}^{\lambda} \right\| i \right\rangle = \left\langle n\omega_f J_f \left\| \hat{T}^{\lambda} \right\| n\omega_i J_i \right\rangle = \sum_{k\alpha k\beta} OBDM(f, i, k_\alpha, k_\beta, \lambda) \left\langle k_\alpha \left\| \hat{T}^{\lambda} \right\| k_\beta \right\rangle \quad (6)$$

where K_i and K_f denote the single-particle states associated with the initial and final model space configurations ($nw_i\ J_i$) and ($nw_f\ J_f$), respectively. The various basis states with the same J value can be recognized by the ω indices. The OBDM in the proton-neutron formalism is shown as [9]:

$$OBDM(f, i, k\alpha, tz, k\beta, tz, \lambda) = \frac{\left\langle n\omega fJf \left\| \left[a_{k\alpha,tz}^+ \otimes \tilde{a}_{k\beta,tz}\right]^{\lambda} \right\| n\omega iJi \right\rangle}{\sqrt{2\lambda+1}} \quad (7)$$

with the isospin projection defined as t_z =1/2 for neutron and t_z = -1/2 for proton.

The one- and two-neutron separation energies, $S_n(Z,N)$ and $S_{2n}(Z,N)$, respectively, are defined as [10,11]:

$$S_n(Z, N) = E_b(Z, N) - E_b(Z, N-1) \quad \textbf{(8)}$$

$$S_{2n}(Z, N) = E_b(Z, N) - E_b(Z, N-2) \quad \textbf{(9)}$$

2.2. Quadrupole Deformation

Nuclei with magic numbers of protons or neutrons with a "closed shell" have a spherical shape. Nuclei with protons or neutrons away from a magic number are generally deformed. The simplest deformation is the quadrupole deformation in which the nuclei may take an oblate shape (cushion) or prolate shape (rugby ball). The deformation parameter is associated with the intrinsic quadrupole moment $\hat{Q}$ as, $\langle\hat{Q}\rangle$given by the following relation [12,13]:

$$\langle\hat{Q}\rangle = \sqrt{\frac{16\pi}{5}} R^2 Y_{20}(\vec{r}) = 2z^2 - r^2 \quad \textbf{(10)}$$

where z and r are the position coordinates of kth nucleon, and r is given in Cartesian coordinates as $r^2=x^2+y^2+z^2$. $\beta 2$ is denoted as the deformation parameter that defines the amount of deformation present in the nucleus [12,13]:

$$\beta_2 = \frac{\sqrt{5\pi}}{3} \frac{\langle\hat{Q}\rangle}{A\langle R^2\rangle} \quad (\mathbf{11})$$

where A is the number of nucleons and R is the nuclear radius.

3. Results and Discussion

The OBDM elements employed in the present study were calculated using the SM code NUSHELLX@MSU [9]. This package comprises a set of wrapper codes that deploy data files for the SM and Hamiltonian inputs to generate the necessary inputs for NUSHELLX. It is a computer codes which utilize to obtain accurate energies and low-lying state spectroscopic overlap in the matrix calculations of the SM Hamiltonian. Also, it utilizes the basis of the J-coupling proton-neutron and the matrix of the J-scheme.

3.1. Radii of Nuclei

Fig. 1a presents the calculated nuclear charge density distributions ρ_{ch} (r) for the Hg-isotopic sequence spanning ^{180}Hg through ^{192}Hg, plotted as a function of the radial distance r(fm). The vertical axis represents the charge density in units of fm^{-3}, ranging from 0 to approximately 0.07 fm^{-3}, while the horizontal axis extends from r = 0 to r ≈ 112 fm with an 8 fm offset. All isotopes exhibit the canonical nuclear charge density profile characteristic of heavy nuclei, a well-defined central saturation plateau near r ≈ 0, succeeded by a smooth surface diffuseness region and a rapid exponential falloff at the nuclear periphery.

The central densities are stable throughout the chain at $\rho_{ch}(0) \approx 0.05$–$0.07$ fm^{-3}, which is in line with the saturation of nuclear matter. With the increment of the mass number, a systematic outward displacement of the surface diffusiveness region can be observed, and this indicates the progressive increase in the nuclear charge radius as additional neutrons populate the valence shell. Interestingly, the occurrence of small, yet physically significant, differences in the tail region of the density profiles of the light isotopes ($^{180\text{-}184}$Hg) is in line with the beginning of increased quadrupole deformation corresponding with the well-known shape coexistence phenomenon in this sub-lead transitional region. The heavier isotopes ($^{190\text{-}192}$Hg) have slightly broader surface diffuseness profiles, as they have larger nuclear charge radii and are slowly transitioning towards more spherical ground-state configurations near the N=112 neutron subshell closure [14,15].

Fig. 1b shows the calculated radial nucleon density distributions, ρ(r), for isotopic chain $^{180\text{-}192}$Hg, based on self-consistent Skyrme Hartree-Fock calculations using the Skxcsba parametrization. The figure is presented as a concatenated plot to enable a systematic comparison of the density profiles over a wide range of neutron numbers, between the neutron-deficient ^{180}Hg (N=100) and the neutron-rich ^{192}Hg (N=112). The isotopes all have a central density of about $\rho_0 \approx 0.16\pm0.01$ fm, which corresponds to the empirical nuclear saturation density.

The fact that this depletion continues up to ^{186}Hg suggests that the Z=80 shell gap is strong even far from stability, and that the $S_{1/2}$ state is weakly admixed with other orbitals even when deformation has begun. This observation provides a complementary test of the shell evolution in the lead region. The nuclear matter density distributions calculated for $^{180\text{-}192}$Hg isotopic chain within Skyrme Skxcsba self-consistent Hartree-Fock frameworks showing salient feature expected of the neutron-deficient heavy nuclei, a strong central saturation density near the empirical value of $\rho_0 \approx 0.16$ fm^{-3}, a gradual increase in nuclear size with mass number A as evidenced by the outward displacement of the half-density radius and a gradual broadening of the surface diffuseness regime in the heavier members of the chain.

Fig. 1c displays the proton density distribution as a function of the radial distance r(fm), covering the ^{180}Hg to ^{192}Hg isotopic chain. The primary feature along the Hg isotopic chain is the central depression for r < 6 fm. Saturation was observed approximately for r ≈ 0.065-0.070 fm. The proton distributions exhibit a minor change in the central region, which is consistent with the fact that the proton number (Z=80) is constant. However, small alterations in the surface region are due to core polarization effects caused by the addition of valence neutrons.

Fig. 1d displays the neutron density distribution of Hg isotopes as a function of radial distance r(fm). In contrast to the proton distribution, neutron densities exhibit a clear regular progression as mass increases. The central density values range from around 0.080 to 0.09 fm. The nuclear radius clearly expands when more neutrons are introduced into the system. The density profiles move toward greater radial distances, indicating the gradual formation of a neutron skin.

These results validate the predictive reliability of the adopted functional for nuclear structure observables in the Z = 80 sub-lead region and provide a self-consistent microscopic basis for interpreting the isotopic evolution of nuclear radii and neutron skin thicknesses. The sensitivity of the surface density profiles to deformation and pairing effects underscores the necessity of extending the present analysis toward beyond-mean-field frameworks to achieve a fully quantitative treatment of shape coexistence and configuration mixing in this isotopic region [16-18].

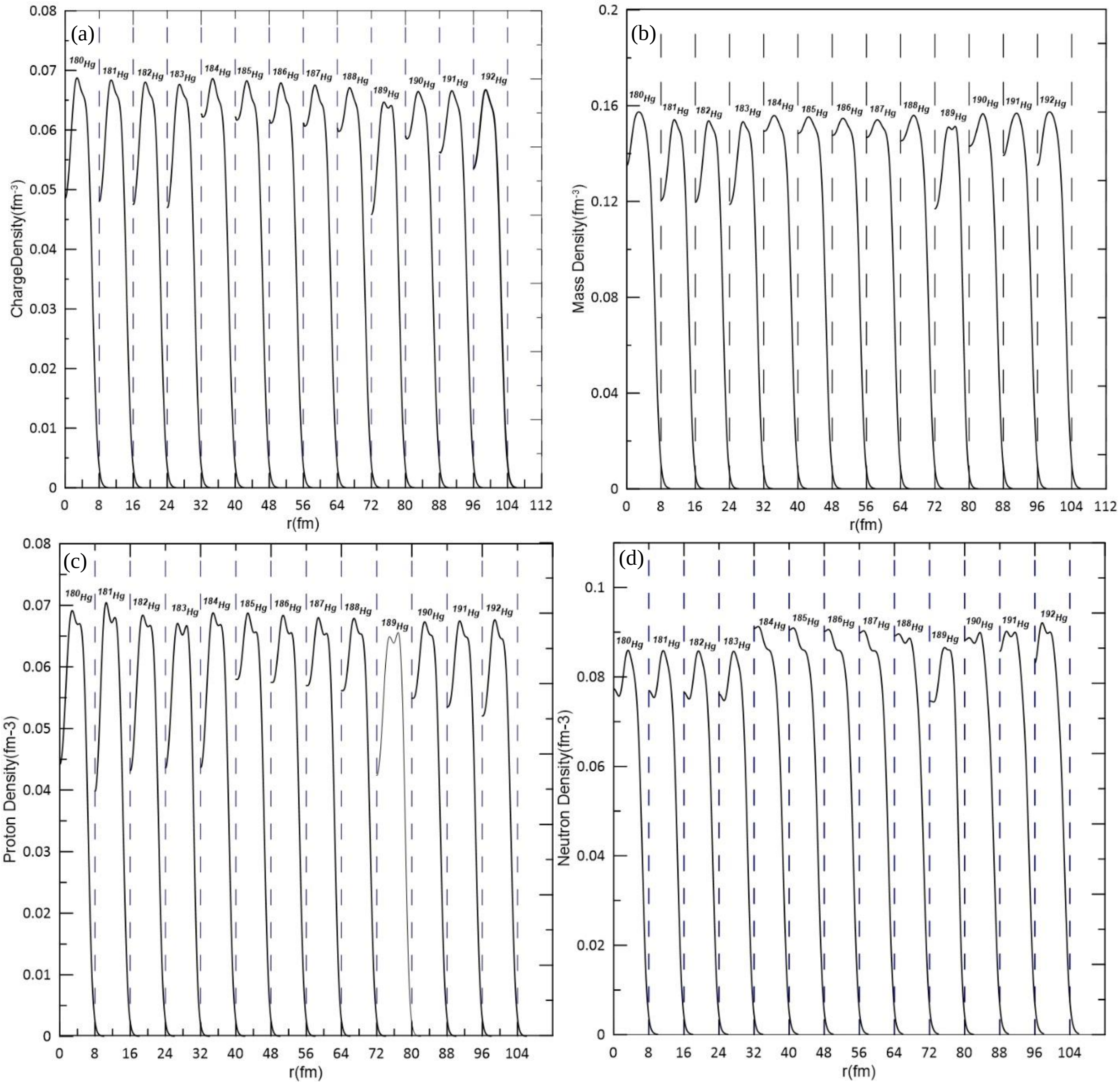

Figure 1: Theoretical nuclear density distributions for Hg isotopes obtained via Skxcsba parameterization. Panel (a) displays the charge density distributions, panel (b) illustrates the mass density distributions, panel (c) displays the Proton density, and panel (d) displays the Neutron density. All in units of fm^{-3}. Starting from ^{180}Hg, isotopic curves are sequentially offset along the x- axis by 8 fm to avoid overlap.

Table 1 presents the rms charge radii and neutron skin for the $^{180-192}$Hg isotopic chain. The results reveal that the SHF calculation deploying the *Skxcsba* parameterization underestimates the experimental charge radii by approximately 0.02−0.082 fm (corresponding to a relative deviation of 0.43-14.52%), yet successfully reproduces the experimental data. The results reveal that the ^{182}Hg to ^{186}Hg isotopes give an indication of shape coexistence and a clear nuclear deformation in this region. The SHF model, while delivering a smooth linearity, lacks the shell-correction sensitivity essential to fully capture the shape-staggering effect. In addition, the neutron skin Δr_{np} gradually increased for the Hg isotopic chain from 0.009 to 0.045 fm, which reflects the accumulation of excessive neutron along the nuclear surface as neutron number progressively increased.

Table 1: The calculated rms charge radius in fm for Hg isotopes, obtained using SHF with Skxcsba parameterization, compared with the experimental data taken from Angeli and Marinova [19].

Isotope	Exp. Charge radii(fm)	Theo. Charge radii (fm)	Exp. Neutron skin Δr_{np} (fm)	Theo. Neutron skin Δr_{np} (fm)
^{181}Hg	5.4364	5.354	0.0032	0.009
^{182}Hg	5.3833	5.358	0.0052	0.004
^{183}Hg	5.4405	5.363	0.0031	0.002
^{184}Hg	5.3949	5.367	0.0047	0.007
^{185}Hg	5.4397	5.371	0.0031	0.012
^{186}Hg	5.4017	5.376	0.0043	0.017
^{187}Hg	5.4046	5.38	0.0042	0.022
^{188}Hg	5.4085	5.385	0.004	0.027
^{189}Hg	5.410	5.389	0.004	0.031
^{190}Hg	5.4158	5.393	0.0037	0.036
^{191}Hg	5.4171	5.398	0.0037	0.04
^{192}Hg	5.4232	5.402	0.0035	0.045

Fig. 2 shows the calculated root-mean-square rms proton radius (R_p, solid circles) and neutron radius (R_n, open squares) of the mercury Hg isotopic chain with respect to mass number A, in the range of A = 180-192. Both quantities are obtained using the Skyrme-Hartree-Fock (SHF) framework that uses the Skxcsba effective interaction. The neutron rms regularly increases in the chain compared to the proton rms, and this is due to the successively increasing neutron excess N >> Z. The difference between R_n and R_p is a direct measure of the neutron skin thickness, $\Delta r_{np} = R_n - R_p$, which is a fundamental measure important in nuclear structure.

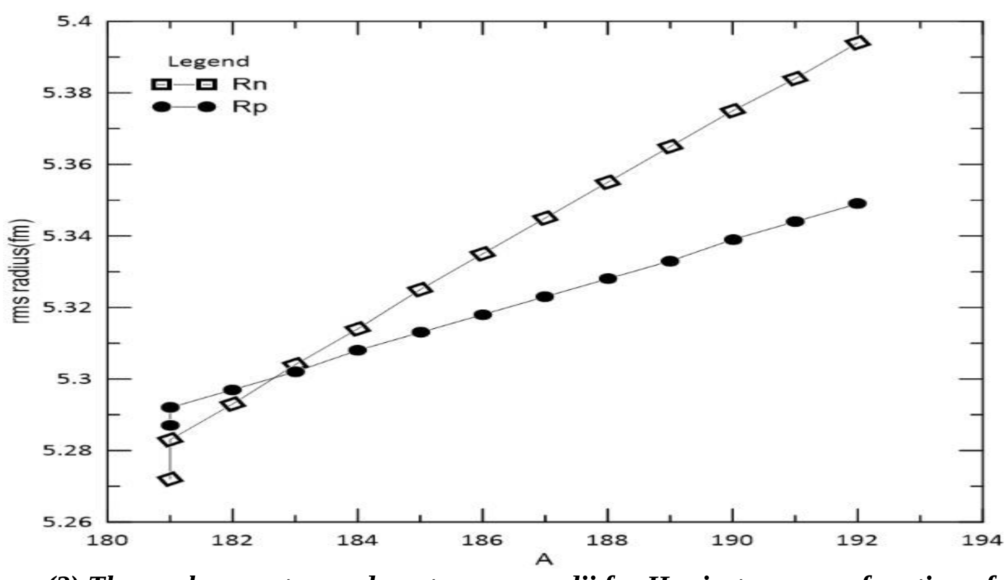

Figure (2) The nuclear proton and neutron rms radii for Hg- isotopes as a function of nucleon number A.

3.2. Binding Energy and Separation Energies

Fig. 3 shows two complementary plots of nuclear binding energy of the Hg isotopic chain spanning A = 180–192. The total binding energy B.E (MeV) is shown in the left panel as a function of mass number A, ranging between 1400 to 1520MeV. On the right panel, the binding energy per nucleon B.E/A (MeV/nucleon) in the same isotopic range, 7.78-7.94 MeV/nucleon. Theoretical predictions using the SHF framework are compared to available experimental data in both panels that are available in evaluated nuclear mass compilations. In the left panel, there is a monotonically increasing and almost linear dependence of the total binding energy on mass number A.

The almost perfect linearity of the B.E curve proves that in this range of isotopes the incremental binding per added neutron is more or less a constant, showing stable bulk nuclear matter properties with no sudden shell or deformation-induced discontinuities [21]. The B.E/A curve in the right panel has a slightly rising tendency from ≈ 7.80 MeV/nucleon at A = 180 to ≈ 7.91 MeV/nucleon at A = 192, interspersed with a prominent staggering between the odd and even levels, over the general ascending slope. This staggering is representative of the role played by the nuclear pairing correlations for even-A isotopes, which have the full benefit of the condensation energy of pairing and always have higher B.E/A values compared to their odd-A neighbors, which supports the persistence of strong neutron pairing across the Z = 80 isotopic chain.

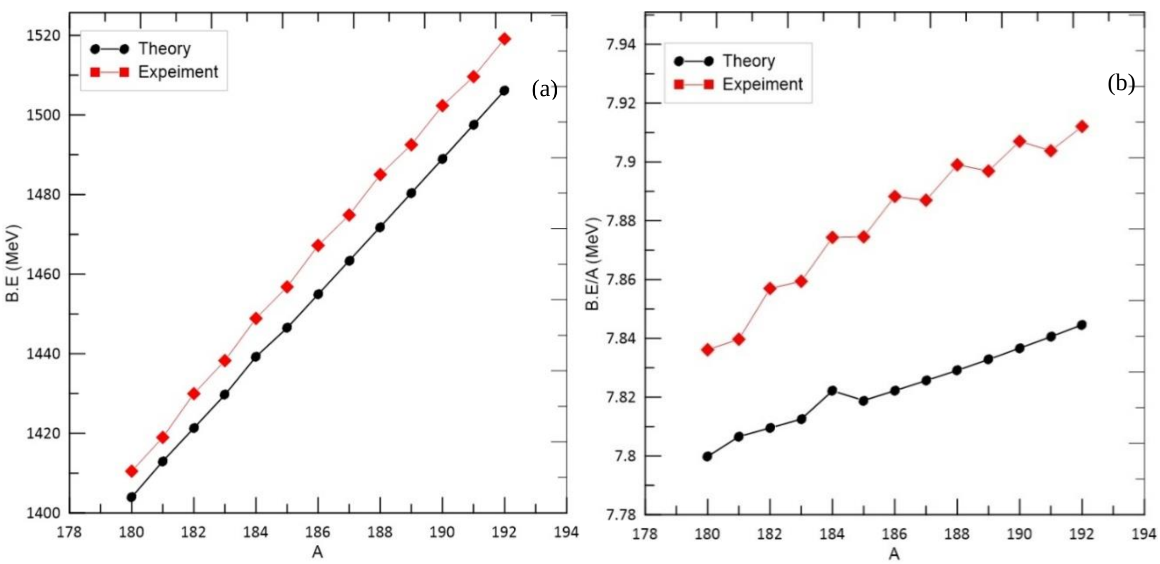

Figure 3: Binding Energy for Hg isotopes as a function of mass number (a)total binding energy (B.E, in MeV) (b) binding energy per nucleon (B.E/A; MeV) plotted as a function of mass number A [20].

Fig. 4 shows the one-neutron separation energies (S_n, panel a) and two-neutron separation energies (S_{2n}, panel b) of the neutron-deficient mercury Hg isotopic chain as a function of mass number A, spanning the range A = 180-192. Both panels show two parallel datasets: theoretical values obtained using the Skyrme Hartree-Fock (SHF) framework with the Skxcsba effective interaction (SHF, represented by red squares linked by solid lines) and experimentally obtained values (Exp., black circles) obtained by the various existing nuclear data compilations. The ordinate in panel (a) spans $S_n \approx 7.5$–11.5 MeV, whereas panel (b) covers $S_{2n} \approx 16.4$–19.6 MeV, both expressed in units of MeV.

The odd-A isotopes systematically yield lower S_n values than their even-A counterparts, as expected of the energy profile of an unpaired valence neutron in the nuclear mean field. The oscillatory amplitude is high, at approximately 1.520 MeV, which is a strong indication of pairing gaps in the Z = 80 region. In panel (b), by contrast, exhibit a smooth and monotonic decreasing pattern of the two-neutron separation energies with increasing A, interrupted by an evident inflection near A=186-188. This structural kink is physically important in that it signals a transitional change in the underlying nuclear mean field that most likely is connected with the development of increased quadrupole collectivity or restructuring of the single-particle level density of the neutron-deficient sub-lead region [22]. Throughout the isotopic sequence, the one-neutron separation energy profile in Fig. 4a exhibits a pronounced odd-even staggering pattern, constituting a hallmark signature of nuclear pairing correlations. As with previous observations, odd-A isotopes are systematically lower in S_n than their even-A counterparts, consistent with the energetic penalty of having an unpaired neutron in the nuclear mean field in the valence shell. The oscillatory amplitude is large, with inter-isotope differences of about 1.520 MeV, which clearly indicate the strength of pairing gaps in Z=80.

In Fig. 4b, both the two-neutron separation energies exhibit a monotonically decreasing, smooth trend with increasing A, with an inflection that can be observed clearly around A = 186-188. Such a structural kink carries a physical implication, namely indicating a transitional change of the underlying nuclear mean field most likely to be identified with the development of increased collectivity of the quadrupole or a redistribution of the single-particle level density of the neutron-deficient sub-lead region. The systematic decrease in neutron binding due to the evolution in nuclear configuration across the isotopic chain is reflected in the near-linear decrease of S_{2n} to larger mass numbers. The general agreement between the SHF prediction and the experimental data across the range of investigation is extremely satisfactory. Fig. 4a shows that the theoretical curve accurately reproduces the phase, as well as the amplitude, of the odd-even staggering, showing that pairing correlations are quantitatively captured using the Skxcsba parameterization, in the $Z = 80$ region. The calculated values of S_{2n} closely trace the experimental descent, with deviations at isolated mass numbers not more than ≈ 0.3 MeV. These remaining discrepancies can be explained by configuration-mixing effects and beyond-mean-field correlations that are not represented by the current framework.

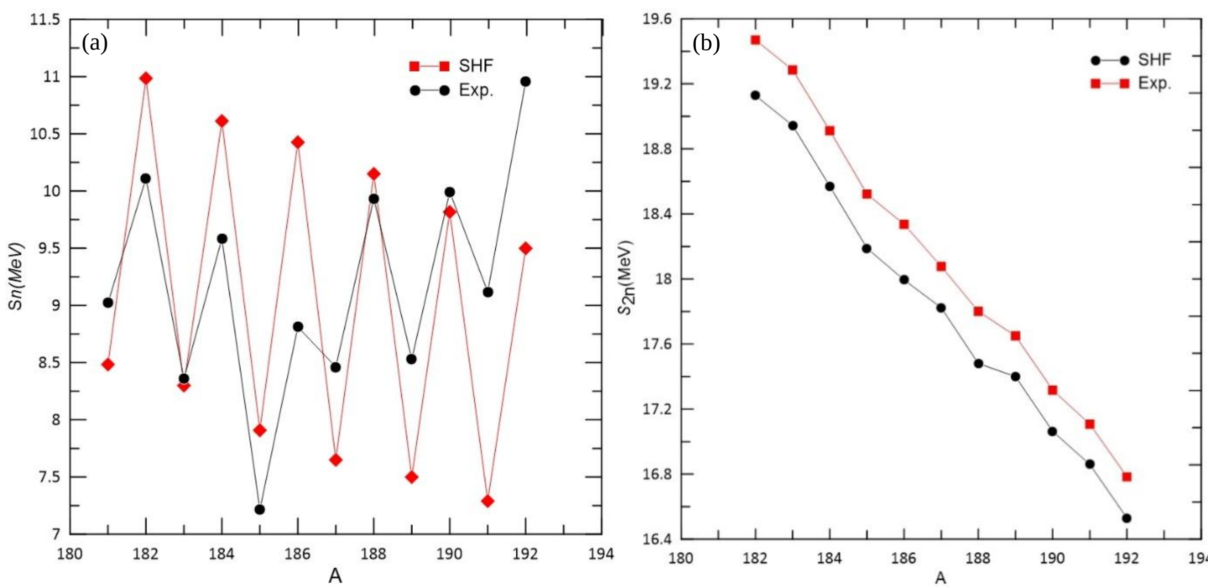

Figure 4: One-neutron (a) and two-neutron (b) separation energies as a function of nucleon number (A) for Hg isotopes.

3.3. Deformation Energy

Fig.5a presents the PES of neutron-deficient even-A mercury isotopes spanning ^{180}Hg to ^{192}Hg, calculated using the Hartree-Fock-Bogoliubov (HFB) methodology with the Skyrme interaction with the HFODD Code. The PES curves trace the total nuclear binding energy B.E (MeV) as a function of the quadrupole deformation parameter β_2, with negative values indicating oblate shapes and positive values indicating prolate geometries. The calculations of the lightest chain members ^{180}Hg, ^{182}Hg, ^{184}Hg, and ^{186}Hg all give an oblate ground-state minimum at near $\beta_2 \approx -0.15$ to -0.20. This is a deformation of about 15-20% away from sphericity, and the associated binding energy minima are the deepest across the whole chain, ^{180}Hg reaching around −1516 MeV and ^{182}Hg settling near −1509 MeV. The narrow width and well-defined depth of these oblate wells are indicative of structurally robust oblate deformation, which derives its stability from the specific shell structure produced by the large number of neutron holes below the N = 126 shell closure. One similarity of all four of these lighter isotopes is that they have a secondary prolate minimum at $\beta_2 \approx +0.25$ to $+0.30$. The secondary well is separated from the oblate ground state by an energy barrier with a height of approximately 2.5 MeV in ^{186}Hg to about 4 MeV in ^{180}Hg. The resulting topology of a double minimum is the typical signal of nuclear shape coexistence, a phenomenon where two or more structurally distinct nuclear structures, each possibly having a qualitatively distinct deformation, coexist at comparable low excitation energies in the same nucleus and form distinct bands of collective states in measured spectra.

The physically most significant change that is observed in the chain is the transition between ^{186}Hg and ^{188}Hg. In this case, the configurations of the oblate and prolate are exchanged effectively. The system switches from an oblate ground state to a predominantly prolate. The prolate side of the PES is very soft at ^{186}Hg, with the secondary prolate minimum less intense and distinct than in the lighter members. At ^{186}Hg, the primary energy minimum becomes the prolate region ($\beta_2 \approx +0.20$), and the previously dominant oblate minimum diminishes to a secondary feature near $\beta_2 \approx -0.15$. The PES of the three heaviest, ^{188}Hg, ^{190}Hg, and ^{192}Hg, has a prolate primary minimum, in the range of $\beta_2 \approx +0.20$ to $+0.25$, and an oblate side only a soft shoulder or a poorly defined secondary well. The prolate minimum deepens from ^{188}Hg to ^{190}Hg and then becomes broader and more diffuse at ^{192}Hg, a trend aligning with the predicted onset regarding neutron subshell closure near N = 126 as predicted by various mean-field models in this mass region. The progressive flattening of the prolate minimum in ^{192}Hg reflects the gradual depletion of neutron pairs occupying the prolate-driving d–g shell orbitals as this subshell closure is approached, which in turn reduces the quadrupole correlation energy responsible for sustaining prolate deformation. The PES of ^{192}Hg also has an exceptionally large-deformation tail extending to $\beta_2 \approx +1.2–1.4$, followed by a steep rise in energy, suggesting a weakly bound superdeformed state in this isotope.

The even-A isotope results establish that neutron-deficient mercury nuclei around the mid-shell region N ≈ 104 host a richly structured energy landscape, and persistent prolate and oblate shape coexistence appears as a strong feature that is not dependent on the particular mean-field parameterization. Although the HFB ground state is mainly prolate-deformed in this range, the marked γ-softness of the oblate minimum suggests that an honest description of the low-lying collective structure requires an explicit description of non-axial degrees of freedom as well as beyond-mean-field correlations. The model-independent reproduction of PES topology as well as the energetic proximity of competing shapes highlights the coexistence of shapes in light Hg isotopes as a robust quantum mechanical phenomenon that is driven by the interplay between a Z = 82 shell closure and a neutron mid-shell collectivity [23,24].

Fig. 5b presents the HFB-calculated PES for the odd-A neutron-deficient mercury isotopes ^{181}Hg, ^{183}Hg, ^{185}Hg, ^{187}Hg, ^{189}Hg, and ^{191}Hg. The horizontal axis spans the deformation parameter β_2 from approximately −0.6 to +1.4, while the vertical axis displays total binding energy in MeV, ranging from about −1380 MeV for ^{191}Hg (least bound) to roughly −1520 MeV for ^{181}Hg (most bound). The covered neutron numbers span N = 101 (^{181}Hg) through N = 111 (^{191}Hg), all lying within the shell region bounded by N = 82 and N = 126. Each of the six isotopes has a multi-minimum deformation structure with two distinctly identified competing configurations. There is a shallow oblate minimum near $\beta_2 \approx -0.15$ to -0.20 in the series and a deeper prolate minimum at $\beta_2 \approx +0.20$ to $+0.35$. In the lighter members of the series (^{181}Hg through ^{187}Hg), this prolate minimum is the absolute minimum of energy, which is again in line with the dominance of prolate ground states near the mid-shell at N ≈ 104. As the neutron number increases from N = 101 toward N = 111, the prolate minimum progressively shallows while the oblate minimum becomes relatively more competitive. The most notable change in this structure is observed in the heavier odd-A isotopes ^{189}Hg and ^{191}Hg, and indicates the weakening prolate driving force as neutron orbitals above N = 104 are occupied. A wide, flat energy profile of $\beta_2 \approx 0$ suggests strong γ-softness around sphericity and is another common feature of all six curves. Instead of showing a sharp minimum at zero deformation, the nuclei in this region are perturbed by shape fluctuations which are of large amplitude and which interpolate between oblate and prolate geometry. The energy barriers between the competing minima are 0.5-1.5 MeV within the series - small enough to allow quantum tunneling and large shape mixing in the low-lying collective states. Some of the curves have a second shoulder or third minimum visible near $\beta_2 \approx +0.5$ to $+0.7$, and this may indicate the start of superdeformed configurations at very prolate shapes, but these are at 4-6 MeV above the ground state [25]. The entire image in Fig. 5b gives much support to the fact that the persistence of prolate and oblate shape coexistence in the full odd-A mercury chain, ^{181}Hg and ^{191}Hg. The potential energy surface (PES) of these six isotopes is located in the neutron-deficient mid-shell region, where the coexistence of shapes is most pronounced due to the competition between the Z = 82 proton shell closure and the neutron collectivity between N = 82 and N = 126. The systematic isotopic effect - between a well-defined prolate ground state in ^{181}Hg and a more balanced oblate-prolate competition in ^{191}Hg - follows a well-defined structural trajectory indicative of the progressive approach to the N = 126 shell closure [26, 27].

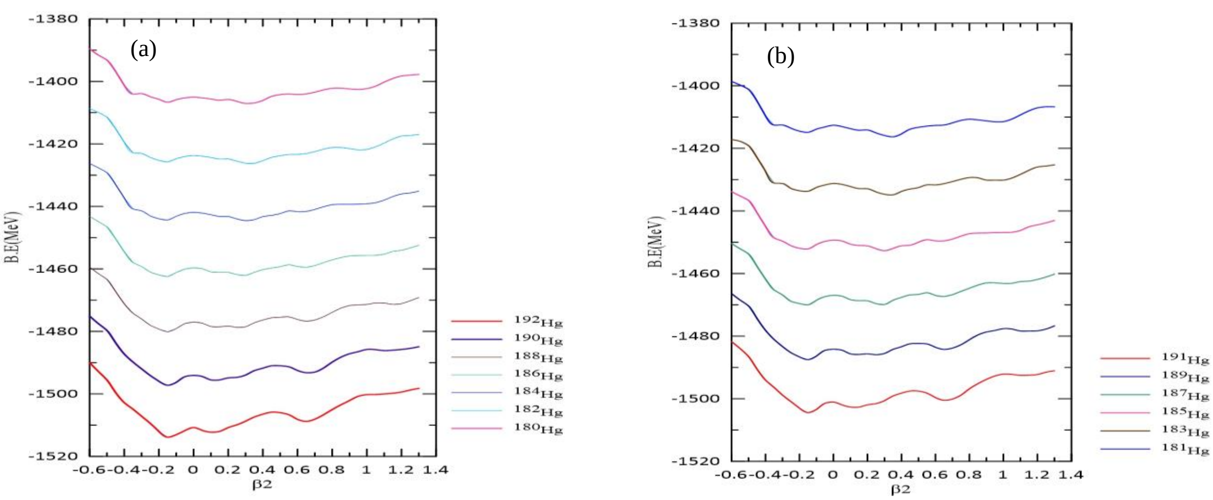

Figure 5: Hg Isotopes deformation energy curves as a function of the quadrupole deformation parameter β2: a) even-even Hg isotopes; b) odd-even Hg isotopes, calculated using HFB with the HFODD code.

4. Conclusions

In summary, the systematic HFB analysis of the $^{180\text{-}192}$Hg isotopic chain successfully described the transition from weakly oblate structures to a prolate-dominated regime near the N=104 neutron mid-shell. The mapping of axial quadrupole potential energy surfaces revealed competing oblate and prolate minima, providing clear evidence of shape coexistence in this region. The barriers separating these configurations became progressively shallower as the neutron number approaches N = 104.

This structural evolution reflects the progressive lowering of proton intruder orbitals from the upper oscillator shell as the neutron mid-shell is approached, thereby weakening the spherical restoring effects associated with the proximity of the Z = 82 proton shell closure. Furthermore, the one-neutron separation energies S_n display pronounced odd–even staggering with an amplitude of approximately 1.5–2.0 MeV, reflecting the influence of neutron-pairing correlations. In contrast, the two-neutron separation energies S_{2n} decreased smoothly from approximately 19.4 MeV at 19.4 MeV at A = 180 to 16.6 MeV. A structural kink near A=186-188 indicated a transition from strongly oblate-deformed configurations to less-deformed ground-state configurations within the mean-field description.

Conflict of Interest

The authors declare no conflicts of interest.

References

1. M. Warda, A. Staszczak, and L. Próchniak, Comparison of Self-Consistent Skyrme and Gogny Calculations for Light Hg Isotopes. *Int. J. Mod. Phys*. E19:787-793(2010). https://doi.org/10.1142/S0218301310015230.
2. A. A. Allami and A. A. Alzubadi, Study of the nuclear structure of some exotic nuclei using nonrelativistic and relativistic mean-field methods. *Int. J. Mod. Phys. E*. **29**(12), 2050090 (2020). https://doi.org/10.1142/S0218301320500901.
3. P. D. Costa, K. Bennaceur, J. Meyer, W. Ryssens, and M. Bender, Impact of choices for center-of-mass correction energy on the surface energy of Skyrme energy density functionals. *Phys. Rev. C*. **109**, 034316 (2024). https://journals.aps.org/prc/abstract/10.1103/PhysRevC.109.034316.
4. W. Ryssens and M. Bender, Skyrme pseudopotentials at next-to-next-to-leading order: Construction of local densities and first symmetry-breaking calculations. *Phys. Rev. C* **104**, 044308 (2021). https://doi.org/10.1103/PhysRevC.104.044308.
5. P. Becker, D. Davesne, J. Meyer, J. Navarro, and A. Pastore, Solution of Hartree-Fock-Bogoliubov equations and fitting procedure using the N2LO Skyrme pseudopotential in spherical symmetry. *Phys. Rev. C*. **96**, 044330 (2017). https://doi.org/10.1103/PhysRevC.96.044330.
6. W. Ryssens, M. Bender, K. Bennaceur, P. Heenen, and J. Meyer, Impact of the surface energy coefficient on the deformation properties of atomic nuclei as predicted by Skyrme energy density functionals. *Phys. Rev. C*. **99**, 044315 (2019). https://doi.org/10.1103/PhysRevC.99.044315.
7. S. H. Mohammed and A. A. Alzubadi, A Study of Nuclear Shape Coexistence Near the Fifth Island of Inversion Using the Hartree–Fock plus Bardeen–Cooper–Schrieffer Method, *J. Eng.* **32**(7), 210 (2026). https://doi.org/10.31026/j.eng.2026.07.11.
8. J. Bartel, H. Molique, B. Nerlo-Pomorska, M. Warda, and K. Pomorski, Search for shape isomers in the Pt-Hg-Pb region, *Phys. Rev. C*. **112**, 064301(2025). https://doi.org/10.1103/gk8b-jl6y.
9. B. A. Brown, *Lecture Notes in Nuclear Structure*. Physics National Superconducting Cyclotron Laboratory and Department of Physics and Astronomy, Michigan State University, E. Lansing, MI 48824 (2005) (unpublished).
10. A. Bohr and B. R. Mottelson, *Nuclear Structure*. Vol. 1, Singapore:World Scientific, 1988.
11. P. J. Brussard and P. W. M. Glaudemans, *Shell Model Applications in Nuclear Spectroscopy*. Elsevier, North-Holland Publishing Company, 1977.
12. P. Ring and P. Schuck, *The Nuclear Many Body Problem*. Germany: Springer Berlin Heidelberg, 2004.
13. D. J. Rowe, *Nuclear Collective Motion Models and Theory*. Singapore: World Scientific, 2010.

14. A. A. Alzubadi and R. A. Allawi, Investigation of the magicity in some even–even Ca isotopes by using shell model and Hartree–Fock–Bogoliubov method. *Indian J Phys,* **96**(4), 1205 (2022). https://doi.org/10.1007/s12648-021-02052-x.
15. A. A. Alzubadi and A. A. Abdulhasan, Nuclear deformation study using the framework of self-consistence Hartree-Fock-Bogoliubov. *Karbala Int. J. Mod. Sci.* **1**(2), 110 (2015). https://doi.org/10.1016/j.kijoms.2015.09.002.
16. U. Nawaz, M. Rajput, S. Singh, G. H. Bhat, A. Bharti and J. A. Sheikh, Theoretical Insights into Nuclear Structure of ^{196}Pt. *EPJ Web of Conferences* **356**, 02021 (2026). https://doi.org/10.1051/epjconf/202635602021.
17. R. N. Bernard, C. Simenel and G. Blanchon, Hartree–Fock–Bogoliubov study of quantum shell effects on the path to fission in ^{180}Hg, ^{236}U and ^{256}Fm. *Eur. Phys. J. A*, **59**(51), 1 (2023). https://doi.org/10.1140/epja/s10050-023-00964-2.
18. P. Morfouace et al., An asymmetric fission island driven by shell effects in light fragments. *Nature.* **641**, 339 (2025). https://doi.org/10.1038/s41586-025-08882-7.
19. I. Angeli and K.P. Marinova, Table of experimental nuclear ground state charge radii: An update. *At. Data Nucl. Data Tables.* **99**(1), 69 (2013). https://doi.org/10.1016/j.adt.2011.12.006.
20. National Nuclear Data Center, Brookhaven National Laboratory, *Nuclear Data*. 2006. https://www.nndc.bnl.gov.
21. A. H. Ali and A. A. Alzubadi, Calculation magnetic dipole moments, electric quadrupole moments and form factors for some Ti isotopes. *Physica Scripta*, **95**(10), 105306 (2020). https://doi.org/10.1088/1402-4896/abbaf4.
22. S. Sakakihara and Y. Tanaka, Oblate-prolate transition in odd-mass light mercury isotopes. *Nucl. Phys. A*. **726**(1-2), 37 (2003). https://doi.org/10.1016/S0375-9474%2803%2901619-1.
23. G. Ulm, S.K. Bhattacherjee et al, Isotope shift of182Hg and an update of nuclear moments and charge radii in the isotope range^{181}Hg-^{206}Hg. *Z. Phys. A - Atomic Nuclei.* **325**, 247 (1986). https://doi.org/10.1007/BF01294605.
24. T. Niksic, D. Vretenar, P. Ring and G. A. Lalazissis, New relativistic mean-field interaction with density-dependent meson-nucleon couplings. *Phys. Rev. C.* **71**, 024312 (2005). https://doi.org/10.1103/PhysRevC.71.024312.
25. K. Nomura, R. Rodriguez-Guzman, L. M. Robledo and H. Abusara, Structure of krypton isotopes within the interacting boson model derived from the Gogny energy density functional. *Phys. Rev. C.* **96**, 034310 (2017). https://doi.org/10.1103/PhysRevC.96.034310.
26. P. F. Mahmood and A. H. Taqi, Deformation and shape transition of even-even tin isotopes using skyrme HFB method. *AIP Conf. Proc*. **2398**, 020044 (2022). https://doi.org/10.1063/5.0093384.
27. P. Sarriguren, R. Rodriguez-Guzman, and L.M. Robledo, Shape transitions in neutron-rich Yb, Hf, W, Os, and Pt isotopes within a Skyrme Hartree-Fock + BCS approach. *Phys. Rev. C*. **77**, 064322 (2008). https://doi.org/10.1103/PhysRevC.77.064322.

التركيب النووي وخصائص التشوه لنظائر الزئبق الغنية بالنيوترونات 180-192 باستخدام طريقة سكايرم-هارتري-فوك

لمى جمال عباس[1]

[1]قسم الطاقة المتجددة، كلية علوم الطاقة والبيئة، جامعة الكرخ للعلوم، بغداد، العراق

الخلاصة

تُجري هذه الدراسة بحثًا حول البنية النووية للحالة الأرضية لنظائر الزئبق (Hg) التي تعاني من نقص النيوترونات في نطاق العدد الكتلي A=180-192 ضمن إطار عمل سكايرم-هارتري-فوك المتسق ذاتيًا (SHF) باستخدام معلمات مختلفة. وتمّ فحص أعضاء السلسلة النظائرية ذات العدد الكتلي A الزوجي-الزوجي والفردي-الزوجي من حيث التشوهات النووية، ونصف قطر الشحنة، وطاقات الربط، وطاقات الفصل، وتوزيعات الكثافة النووية. وقد توافقت أنصاف أقطار الشحنة المحسوبة مع المنهجية التجريبية، بانحرافات متبقية أقل من 0.082 فيمتومتر، مما يؤكد الموثوقية الكمية لنموذج SHF في وصف المتغيرات المكانية النووية. علاوة على ذلك، أظهرت توزيعات كثافة الشحنة النووية المحسوبة باستخدام نموذج سكيرم Skxcsba توافقًا جيدًا مع البيانات التجريبية المتاحة، حيث بلغت الكثافة المركزية حوالي $\rho_{ch} \approx 0.06–0.07\ fm^{-3}$، مع انزياح خارجي منتظم مع ازدياد العدد الكتلي. وتؤكد ملامح كثافة المادة النووية التشبع المركزي قرب $\rho_{o} \approx 0.16\ fm^{-3}$، إلى جانب اتساع تدريجي لمنطقة انتشار السطح باتجاه النظائر الأثقل، بما يتوافق مع ازدياد حجم النواة. وتم رسم خرائط أسطح طاقة الوضع الرباعية المحورية (PESs) كدالة لمعامل التشوه β_2 لجميع النظائر المدروسة. وكشفت الأسطح الناتجة عن انتقال من التكوينات المفلطحة بشكل طفيف إلى التكوينات المطاولة قرب منطقة منتصف غلاف النيوترونات.

الكلمات المفتاحية: نظائر الزئبق، التواجد الآني المظهري، سكايرم–هارتري–فوك، التشوه الرباعي، قشرة النيوترون.